Orientational melting in a mesoscopic system of charged particles

Orientational Melting in a Mesoscopic System of Charged Particles

Lucia Duca,[1,2] Naoto Mizukami,[1,2,3] Elia Perego,[1,2,†] Massimo Inguscio,[2,4,5] and Carlo Sias[1,2,4,*]
[1]*Istituto Nazionale di Ricerca Metrologica (INRiM), 10135 Torino, Italy*
[2]*European Laboratory for Nonlinear Spectroscopy (LENS), 50019 Sesto Fiorentino, Italy*
[3]*Politecnico di Torino, 10129 Torino, Italy*
[4]*Istituto Nazionale di Ottica del Consiglio Nazionale delle Ricerche (CNR-INO), 50019 Sesto Fiorentino, Italy*
[5]*Department of Engineering, Campus Bio-Medico University of Rome, 00128 Rome, Italy*

(Received 26 October 2022; revised 4 March 2023; accepted 17 July 2023; published 25 August 2023)

A mesoscopic system of a few particles can undergo changes of configuration that resemble phase transitions but with a nonuniversal behavior. A notable example is orientational melting, in which localized particles with long-range repulsive interactions forming a two-dimensional crystal become delocalized in common closed trajectories. Here we report the observation of orientational melting occurring in a two-dimensional crystal of up to 15 ions. We measure density-density correlations to quantitatively characterize the occurrence of melting, and use a Monte Carlo simulation to extract the angular kinetic energy of the ions. By adding a pinning impurity, we demonstrate the nonuniversality of orientational melting and create novel configurations in which localized and delocalized particles coexist. Our system realizes an experimental testbed for studying changes of configurations in two-dimensional mesoscopic systems, and our results pave the way for the study of quantum phenomena in ensembles of delocalized ions.

DOI: 10.1103/PhysRevLett.131.083602

A system of confined particles with long-range repulsive interactions becomes localized in a self-ordered crystal structure at a sufficiently low temperature. Crystallization of a few particles has been observed in a wide variety of physical systems, including Wigner molecules of electrons in two-dimensional quantum dots [1], trapped ions [2,3], electrons floating in liquid helium [4], atomic clusters [5], vortices in mesoscopic superconducting disks [6], and dusty plasmas [7]. When confined in an isotropic two-dimensional (2D) potential, a mesoscopic crystal can melt in the angular degree of freedom since there is no preferential orientation of the crystal. This orientational melting can be triggered by thermal or quantum fluctuations [8], and results in a delocalization of the particles in concentric circular trajectories (shells), while the system remains localized radially [9–11]. Notably, orientational melting is a change of configuration that resembles a phase transition in a macroscopic system, but out of the thermodynamic limit. As a result, orientational melting is a nonuniversal phenomenon, i.e., it occurs at conditions that strongly depend on the specific properties of the system [12].

Orientational melting has been extensively studied with computer simulations for systems of particles with different types of long-range interaction, e.g., Yukawa [13], dipolar [14], and Coulomb interactions [15,16] by using Monte Carlo and molecular dynamics. More recently, a number of theoretical works have explored the occurrence of orientational melting in more complex scenarios, e.g., in nondegenerate two-dimensional potentials [17], in the presence of local impurities [18], in the case of intershell rotations [19], and in the formation of supersolid states of ultracold atoms [20].

Despite the vast theoretical literature, orientational melting has been observed only in a few pioneering experiments with paramagnetic colloidal spheres [21], charged dust particles [22], and small Coulomb crystals of trapped ions [3,23]. However, a detailed experimental investigation fully revealing the nonuniversal features of orientational melting has been missing so far. Remarkably, theory predicts that for given numbers of particles—called magic numbers—the orientational melting is particularly disfavored [24]. This is a clear signature of the mesoscopic nature of orientational melting, as the presence of magic numbers—which arise from the interplay between fluctuations (either quantum or thermal), interactions, and the external potential—are found in the most diverse mesoscopic systems, e.g., vortices in superconductors [6], electrons in quantum dots [1], colloids [25], and atomic nuclei [26]. Moreover, although some dependence of orientational melting from the number of particles has been observed in dust clusters [22], the identification and characterization of magic numbers in orientational melting have not been experimentally investigated so far.

Here, we directly observe and characterize orientational melting in a two-dimensional crystal of Ba^+ trapped ions. The main advantages of using trapped ions are the possibility of precisely setting the number of particles and of creating two-dimensional crystals by using external electric fields [27–30]. Moreover, we can observe the occurrence of the transition in real time by using fluorescence imaging.

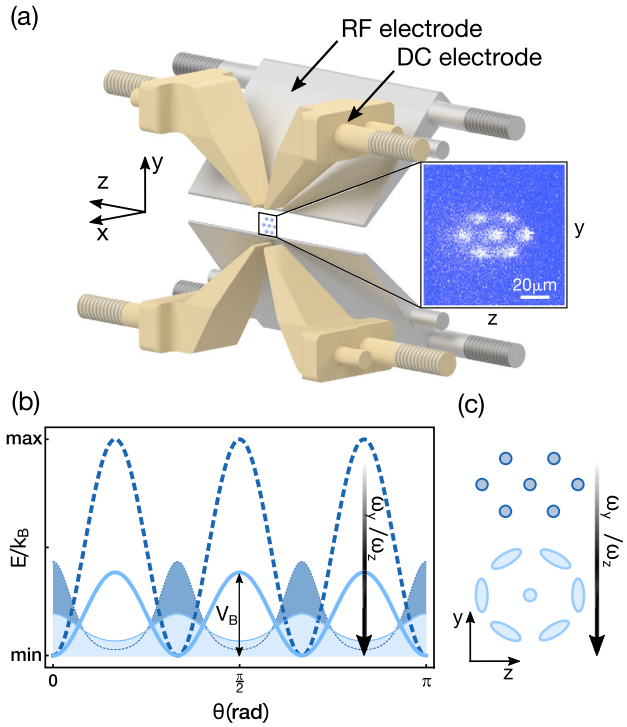

FIG. 1. Sketch of the physical system. (a) The ion trap is composed by 4 rf (gray, only two shown) and 4 dc (yellow) electrodes. The inset shows a picture of a two-dimensional crystal of 7 $^{138}Ba^{+}$ ions in a potential with trap frequencies $(\omega_x, \omega_y, \omega_z) = 2\pi \times (400, 121, 97)$ kHz. (b) A reduction of the ω_y/ω_z ratio towards unity corresponds to a decrease of the height V_B of the potential barrier associated to the rigid rotation of the crystal. When V_B is reduced, e.g., when the angular periodic potential changes from deep (dashed dark blue) to shallow (solid light blue), the particles spatial distribution spreads as illustrated in the figure by the two light and dark blue shaded thermal distributions and their corresponding sketches in (c). When the barrier is further lowered, the particles undergo orientational melting.

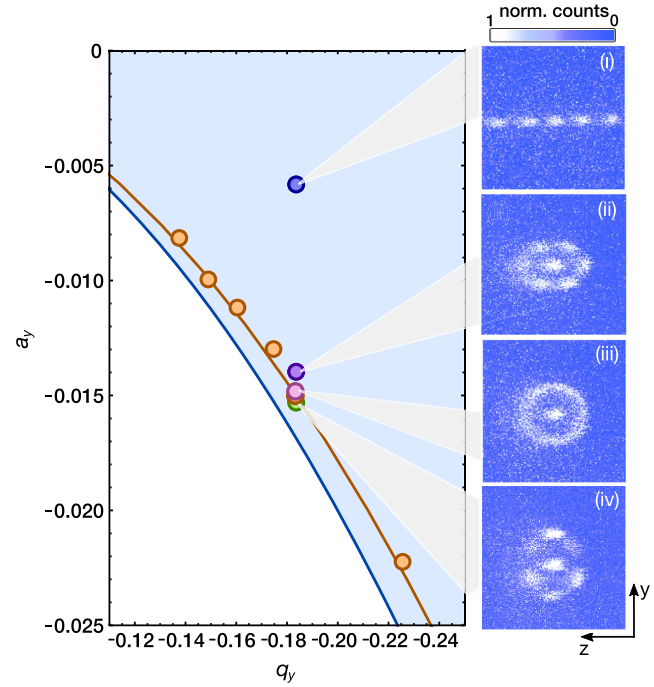

FIG. 2. Accessing orientational melting by changing the particles' confining potential. Left: stability diagram of the ion trap calculated for $^{138}Ba^{+}$, expressed as a function of a_y and q_y [31]. The yellow curve corresponds to the condition $\omega_y/\omega_z = 1$, as expected from the simulation of our trap, and fits inside the stability region (blue area). The location of this curve is confirmed by experimental data (yellow dots) obtained from fitting the ions' spatial distribution and corresponding to a radially symmetric crystal [31]. Right: images of 5 (i) and 7 (ii)–(iv) $^{138}Ba^{+}$ ions at $q_y = -0.182$ and different values of a_y. The images illustrate how crystallization and ellipticity change as a function of a_y across the melting transition. The images are taken at $\omega_y/\omega_z = (3.9, 1.2, 1.1, 0.9)$, $\omega_y = 2\pi \times (246, 121, 107, 91)$ kHz, and $q_y = -0.182$, top to bottom.

Our system consists of N singly charged particles confined in a two-dimensional harmonic potential. The Hamiltonian describing this system is

$$H = \sum_{i=1}^{N} \left(\frac{\mathbf{p_i}^2}{2m_i} + \frac{m_i}{2}(\omega_y^2 y_i^2 + \omega_z^2 z_i^2) + \sum_{j>i}^{N} \frac{\alpha}{|\mathbf{r_i} - \mathbf{r_j}|} \right), \quad (1)$$

where N is the total number of ions, m_i is the ion mass, $\mathbf{r_i} = (y_i, z_i)$ is the position of the ith ion in the two-dimensional y-z plane with trap frequencies ω_y and ω_z, $\mathbf{p_i}$ is the ith ion momentum, $\alpha = e^2/(4\pi\epsilon_0)$, e is the electron charge, and ϵ_0 is the vacuum permittivity. The Hamiltonian in Eq. (1) is well approximated by the pseudopotential created by the Paul trap shown in Fig. 1(a). We do not consider micromotion, whose effects result in a minor correction [31]. The trap frequencies depend on the voltages applied to the rf and dc electrodes, $V_{\rm rf}$ and $V_{\rm dc}$, respectively, and can be expressed in terms of the Mathieu parameters $\mathbf{a}$ and $\mathbf{q}$ [37]. We can continuously change the ratio ω_y/ω_z by varying $V_{\rm dc}$ while keeping the dynamics in two dimensions, i.e., $\omega_x \gg \omega_y, \omega_z$ [31,38]. In this potential, the Doppler cooled ions self-arrange in a 2D crystal with elliptical shape resulting from the anisotropy of the trap, see Fig. 1(a). Figure 1(b) shows the energy of the system as the crystal is rigidly rotated by an angle θ from its equilibrium position. This energy has for $\omega_y \simeq \omega_z$ a sinusoidal shape with amplitude $V_B/2$ [24,31,39]. The ions are localized when V_B is much higher than the ions' kinetic energy along the angular direction (or angular kinetic energy) E_T, while the ions' angular distribution starts spreading when V_B becomes comparable to E_T [see Figs. 1(b) and 1(c)].

We access the melting transition by varying $\mathbf{a}$ and $\mathbf{q}$ (see Fig. 2).When $|\mathbf{a}|$ is increased, the ion crystal shape changes from a line to an ellipse (i)–(ii). When $\omega_y/\omega_z \simeq 1$, we observe orientational melting as the ions displace along a

circular trajectory (iii). Crystallization recovers when $|\mathbf{a}|$ is further increased (iv). This is a clear indication that the loss of crystallization is not caused by trivial effects like instabilities arising at the edge of the stability diagram [40] or excess micromotion [41]. We note that melting occurs for all the pairs of parameters $(\mathbf{a}, \mathbf{q})$ for which $\omega_y/\omega_z = 1$.

To quantitatively characterize the onset of melting, we image the ions as we continuously vary ω_y/ω_z while $q_y = -0.182$ is fixed. Each image records the fluorescence light, and therefore provides a spatial density distribution of the particles over the exposure time. We quantify the loss of angular ordering of the ions by using the angular correlation function

$$g(\Delta\theta) = \frac{\sum_{\theta=0}^{2\pi} n(\theta)n(\theta+\Delta\theta) - \sum_{\theta=0}^{2\pi} n(\theta)^2}{\sum_{\theta=0}^{2\pi} n(\theta)^2}, \quad (2)$$

where $n(\theta)$ is the angular density distribution. $g(\Delta\theta)$ reflects the probability of finding two particles at an angular distance $\Delta\theta$ along an elliptical trajectory enclosing the ions [31]. If the ions form a crystal, $g(\Delta\theta)$ will show a modulation with period $\theta_{NT} = 2\pi/N_T$, where N_T is the number of ions in the elliptical path.

Figure 3(a) shows the amplitude of angular correlations C measured for 4 and 7 $^{138}Ba^+$ ions as a function of ω_y/ω_z. The data show that the crystal loses and retrieves localization as ω_y/ω_z is changed across 1. The change is continuous and the onset of melting is dependent on the ion number, as images (i) and (ii) in Fig. 3(b) illustrate, indicating that the transition has no universal character. We compare the measured angular correlation C with the results from a Monte Carlo simulation for different temperatures (see [31]). The two curves that provide the best fit correspond to an angular kinetic energy of $E_{T4}/k_B = 102$ and $E_{T7}/k_B = 96$ mK for 4 and 7 ions, respectively. These values are comparable with the temperatures of Doppler cooled ion crystals in Paul traps with a similar geometry [42,43]. The comparison with the simulation provides a valid alternative to conventional thermometry methods like sideband spectroscopy and fluorescence lineshape analysis, which would be challenging in our system because of the low energy excitations. Moreover, the radial and axial directions are most likely not in thermal equilibrium [28]. As can be noted from Fig. 3(c), the agreement between data and theory worsen for $\omega_y/\omega_z < 1$. We attribute this to the fact that this region corresponds to the edge of the stability diagram (see Fig. 2) where additional contributions to the dynamics might become relevant for the melting transition [40].

The loss of ordering is associated with a decrease in the localization of each particle, as predicted by computer simulations (see, e.g., Refs. [11,19]). We measure the angular spread σ of the ion density distribution by fitting the density profiles with a multi-Gaussian function [31].

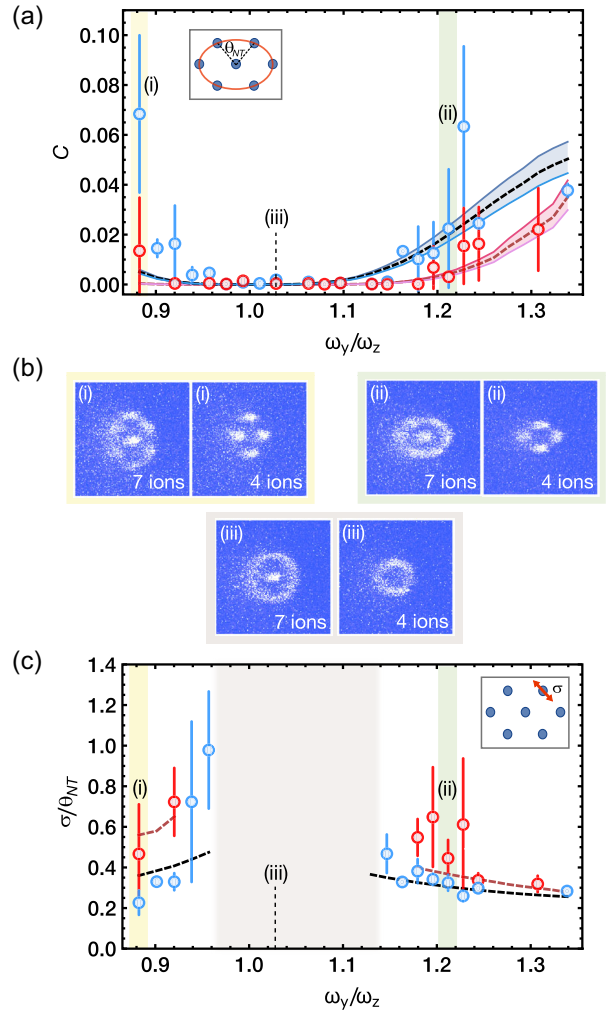

FIG. 3. Characterization of orientational melting for 4 and 7 ions. (a) Amplitude C of the angular density-density correlation function $g(\theta_{NT})$ calculated along the elliptic trajectory (inset). The onset of melting is clearly different for 4 (blue data) and 7 (red data) ions, as shown in the raw images in (b) taken in the regions (i) and (ii). The dashed black (red) line corresponds to the correlation amplitude expected for a crystal of 4 (7) ions at the best fitting temperature of $E_{T4}/k_B = 102$ mK ($E_{T7}/k_B = 96$ mK), as calculated from a Monte Carlo simulation. The blue (red) shaded area for 4 (7) ions represents a change of ± 10 mK from the best fitting curve. (c) Increase of the angular spread σ as the melting transition is approached (see inset). σ is obtained by fitting the density distribution [31], and the values are normalized by the angular separation θ_{NT} between the ions. The gray central area corresponds to trap conditions for which no density modulation is visible, see images (iii) in (b). The dashed black and red lines correspond to the spread of the simulated density profiles for 4 and 7 ions at a temperature E_{T4}/k_B and E_{T7}/k_B, respectively. The error bars in (a),(c) indicate the standard deviation of the mean over 3 to 10 images.

We perform the fit only on the data with $C > 4 \times 10^{-4}$, for which the spatial modulation is non-negligible. Figure 3(c) shows the experimental data and the results of the simulation, which are in good agreement.

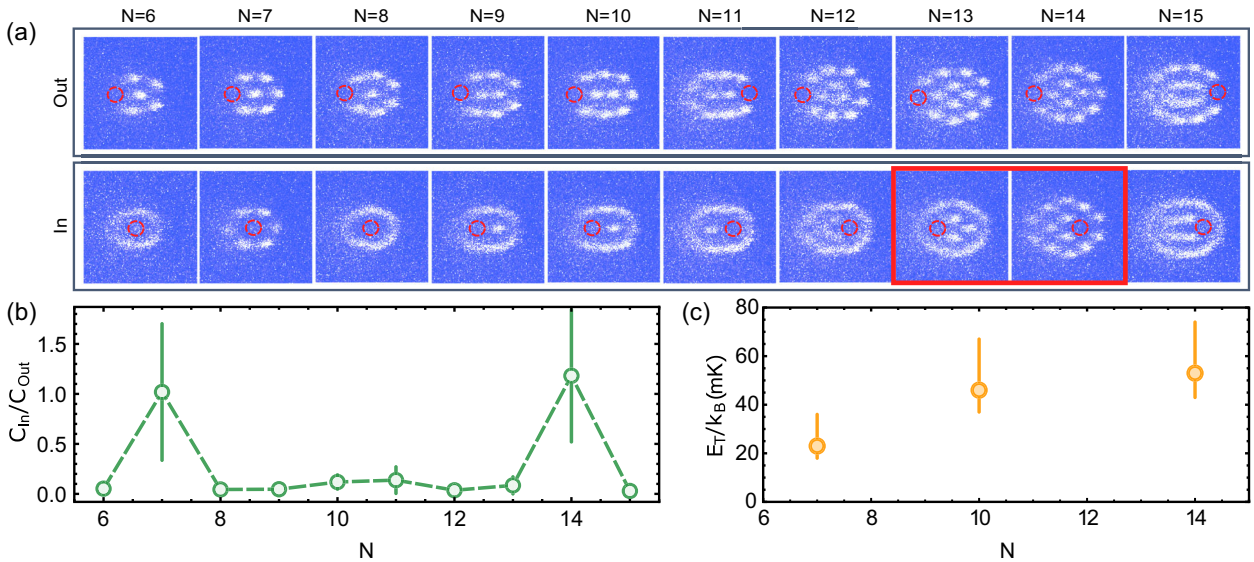

FIG. 4. Orientational melting in the presence of a pinning impurity. (a) Single snapshot images of a crystal of 6 to 15 ions in the presence of an impurity ion of a different isotope. The data are taken at the onset of melting $\omega_y/\omega_z = 1.18$ and $q_y = -0.182$, corresponding to $(\omega_x, \omega_y, \omega_z) = 2\pi \times (401, 116, 98)$ kHz. The impurity appears as a dark ion (red circle). The upper (lower) images correspond to the impurity located in the outer (inner) shell. The impurity ion suppresses melting in the hosting shell (see text and Ref. [31]). (b) We quantify the level of localization for different N by calculating the ratio between the correlations' amplitudes obtained with the dark ion in the inner (C_{In}) and outer shell (C_{Out}) (green dots). The error bars of the data correspond to the standard deviation of the mean, which is calculated on 4 to 18 images depending on N. The dashed line is a guide to the eye. The plot shows that $N = 7$ and $N = 14$ correspond to magic numbers for which the melting transition is disfavored. (c) Angular kinetic energy of the outer ring for $N = 7$, 10, 14. The temperature is extracted by comparing the measured correlations C_{In} and their standard deviations with a Monte Carlo simulation (see text).

We increase the level of control over the occurrence of melting by locally inducing the crystallization of a single shell with the use of a pinning impurity. We realize this scenario, which was suggested in a similar fashion for electrons in a quantum dot [18,44], by deliberately adding one ion of a lighter isotope of Ba^+ that is not resonant to the cooling light [31] [see Fig. 4(a)]. A lighter isotope localizes along the trap z axis as it experiences a larger value of ω_y/ω_z than $^{138}Ba^+$ [31], resulting in an increase of V_B. Therefore, when ω_y/ω_z is set at the crossover of the transition, the impurity inhibits melting of the whole shell where it is located. Figure 4(a) shows the occurrence of melting in a crystal of 6 to 15 ions at the onset of melting ($\omega_y/\omega_z = 1.18$) and in the presence of one impurity. When the impurity is located in the inner shell, the outer shell can still undergo melting, see for example $N = 13$ in Fig. 4(a). This is an evidence that the different shells can behave independently to one another [24,45]. We observe that melting is suppressed for the magic numbers $N = 7$ and $N = 14$. The disparity between $N = 13$ and $N = 14$ cases [red box in Fig. 4(a)] is remarkable, as the inclusion of a single particle alters the entire collective behavior. The emergence of the magic numbers, corresponding to the highest barrier V_B, can be intuitively attributed to two factors. The first is the symmetry of the crystal structure with respect to the trap: the more ions are aligned to the trap weak axis (e.g., in the case of $N = 7$), the higher V_B. The second is the ratio between the number of ions in the inner and outer ring: the furthest this number is from an integer, the lower the friction and hence the barrier V_B [46].

To quantitatively compare the level of localization for different N, we computed the correlation amplitudes in the outer shell for the cases in which the dark ion is in the inner (C_{In}) and outer (C_{Out}) shell. The ratio $C_{\mathrm{In}}/C_{\mathrm{Out}}$ as a function of N is plotted in Fig. 4(b), and clearly shows that the $N = 7$ and $N = 14$ correspond to the most stable crystalline configurations among the ones we explored [16,24]. We compare the measured correlations with our Monte Carlo simulation for $N = 7$, 10, 14. We extract the angular temperature E_T/k_B by least square analysis [see Fig. 4(c)]. We measure an increase in temperature with the size of the crystal, which we interpret as an effect due to the micromotion energy increase out of the center of the trap.

In conclusion, our results illustrate the direct observation of orientational melting in a 2D mesoscopic system of charged particles. We quantitatively characterize the occurrence of melting by measuring density correlations and find excellent agreement with the results of a Monte Carlo simulation, which we use to extract the ions' angular kinetic energy. We observe the presence of magic numbers and inhibit melting by using a single impurity. Our results pave the way for exploring further the thermodynamics of a

few charged particles by looking at quantities like the heat capacity [47], the low-energy excitation spectrum [48] across melting in order to explore its possible phase transition nature [49], and defect formation after quenching [50,51]. Moreover, the experimental control that we achieve shows that our system represents a promising alternative route with respect to ring traps [52,53] for creating charged rotors and controlling them at a quantum level [54], with applications in sensing [55] and in fundamental physics [56,57]. Finally, we note that in the presence of at least two shells and an impurity, orientational melting can be used to study friction between two rotating periodically rugged surfaces [46] with no edges [58,59]. In this context, the number of ions in each shell could be additionally controlled by producing isomeric excitations of the crystal [60].

We gratefully thank Federico Berto, Roberto Concas, and Amelia Detti for their support in the realization of the experimental apparatus. We thank Guido Pupillo, Michael Drewsen, Chiara Menotti, Giovanna Morigi, and the Quantum Gases group at LENS for fruitful discussions. Moreover, we are grateful to Martina Knoop, Boris Blinov, and Guenter Werth for helpful discussions during the assembly of the experimental setup. This project has received funding from the European Research Council (ERC) under the European Union's Horizon 2020 research and innovation programme (Grant Agreement No. 639242). This work was financially supported by the FARE-MIUR grant UltraCrystals (Grant No. R165JHRWR3).

*To whom inquiries should be addressed.
c.sias@inrim.it
†Present address: Department of Physics, University of California, Berkeley, California, USA.

[1] S. M. Reimann and M. Manninen, Electronic structure of quantum dots, Rev. Mod. Phys. **74**, 1283 (2002).
[2] F. Diedrich, E. Peik, J. M. Chen, W. Quint, and H. Walther, Observation of a Phase Transition of Stored Laser-Cooled Ions, Phys. Rev. Lett. **59**, 2931 (1987).
[3] D. J. Wineland, J. C. Bergquist, W. M. Itano, J. J. Bollinger, and C. H. Manney, Atomic-Ion Coulomb Clusters in an Ion Trap, Phys. Rev. Lett. **59**, 2935 (1987).
[4] C. C. Grimes and G. Adams, Evidence for a Liquid-To-Crystal Phase Transition in a Classical, Two-Dimensional Sheet of Electrons, Phys. Rev. Lett. **42**, 795 (1979).
[5] P. Schauss, M. Cheneau, M. Endres, T. Fukuhara, S. Hild, A. Omran, T. Pohl, C. Gross, S. Kuhr, and I. Bloch, Observation of spatially ordered structures in a two-dimensional rydberg gas, Nature (London) **491**, 87 (2012).
[6] I. V. Grigorieva, W. Escoffier, J. Richardson, L. Y. Vinnikov, S. Dubonos, and V. Oboznov, Direct Observation of Vortex Shells and Magic Numbers in Mesoscopic Superconducting Disks, Phys. Rev. Lett. **96**, 077005 (2006).
[7] W.-T. Juan, Z.-H. Huang, J.-W. Hsu, Y.-J. Lai, and I. Lin, Observation of dust coulomb clusters in a plasma trap, Phys. Rev. E **58**, R6947 (1998).
[8] M. Bonitz, P. Ludwig, H. Baumgartner, C. Henning, A. Filinov, D. Block, O. Arp, A. Piel, S. Käding, Y. Ivanov, A. Melzer, H. Fehske, and V. Filinov, Classical and quantum Coulomb crystals, Phys. Plasmas **15**, 055704 (2008).
[9] A. V. Filinov, M. Bonitz, and Y. E. Lozovik, Wigner Crystallization in Mesoscopic 2d Electron Systems, Phys. Rev. Lett. **86**, 3851 (2001).
[10] J. Böning, A. Filinov, P. Ludwig, H. Baumgartner, M. Bonitz, and Y. E. Lozovik, Melting of Trapped Few-Particle Systems, Phys. Rev. Lett. **100**, 113401 (2008).
[11] I. V. Schweigert, V. A. Schweigert, and F. M. Peeters, Radial-Fluctuation-Induced Stabilization of the Ordered State in Two-Dimensional Classical Clusters, Phys. Rev. Lett. **84**, 4381 (2000).
[12] T. L. Hill, *Thermodynamics of Small Systems*, Dover Books on Chemistry (Dover Publications, New York, 1994).
[13] H. Totsuji, C. Totsuji, and K. Tsuruta, Structure of finite two-dimensional Yukawa lattices: Dust crystals, Phys. Rev. E **64**, 066402 (2001).
[14] A. I. Belousov and Y. E. Lozovik, Mesoscopic and macroscopic dipole clusters: Structure and phase transitions, Eur. Phys. J. D **8**, 251 (2000).
[15] V. M. Bedanov and F. M. Peeters, Ordering and phase transitions of charged particles in a classical finite two-dimensional system, Phys. Rev. B **49**, 2667 (1994).
[16] A. I. Belousov and Y. E. Lozovik, Quantum melting of mesoscopic clusters, Phys. Solid State **41**, 1705 (1999).
[17] S. W. S. Apolinario, B. Partoens, and F. M. Peeters, Inhomogeneous melting in anisotropically confined two-dimensional clusters, Phys. Rev. E **74**, 031107 (2006).
[18] A. Ghosal, A. D. Güçlü, C. J. Umrigar, D. Ullmo, and H. U. Baranger, Correlation-induced inhomogeneity in circular quantum dots, Nat. Phys. **2**, 336 (2006).
[19] S. Maity, P. Deshwal, M. Yadav, and A. Das, Dynamical states in two-dimensional charged dust particle clusters in plasma medium, Phys. Rev. E **102**, 023213 (2020).
[20] G. Pupillo, A. Micheli, M. Boninsegni, I. Lesanovsky, and P. Zoller, Strongly Correlated Gases of Rydberg-Dressed Atoms: Quantum and Classical Dynamics, Phys. Rev. Lett. **104**, 223002 (2010).
[21] R. Bubeck, C. Bechinger, S. Neser, and P. Leiderer, Melting and Reentrant Freezing of Two-Dimensional Colloidal Crystals in Confined Geometry, Phys. Rev. Lett. **82**, 3364 (1999).
[22] A. Melzer, A. Schella, J. Schablinski, D. Block, and A. Piel, Instantaneous Normal Mode Analysis of Melting of Finite Dust Clusters, Phys. Rev. Lett. **108**, 225001 (2012).
[23] D. Reiss, K. Abich, W. Neuhauser, C. Wunderlich, and P. E. Toschek, Raman cooling and heating of two trapped Ba^+ ions, Phys. Rev. A **65**, 053401 (2002).
[24] V. A. Schweigert and F. M. Peeters, Spectral properties of classical two-dimensional clusters, Phys. Rev. B **51**, 7700 (1995).

[25] J. Wang, C. F. Mbah, T. Przybilla, B. Apeleo Zubiri, E. Spiecker, M. Engel, and N. Vogel, Magic number colloidal clusters as minimum free energy structures, Nat. Commun. **9**, 5259 (2018).

[26] R. F. G. Ruiz and A. R. Vernon, Emergence of simple patterns in many-body systems: From macroscopic objects to the atomic nucleus, Eur. Phys. J. A **56**, 136 (2020).

[27] T. B. Mitchell, J. J. Bollinger, D. H. E. Dubin, X.-P. Huang, W. M. Itano, and R. H. Baughman, Direct observations of structural phase transitions in planar crystallized ion plasmas, Science **282**, 1290 (1998).

[28] M. D'Onofrio, Y. Xie, A. J. Rasmusson, E. Wolanski, J. Cui, and P. Richerme, Radial Two-Dimensional Ion Crystals in a Linear Paul Trap, Phys. Rev. Lett. **127**, 020503 (2021).

[29] K. Okada, M. Wada, T. Takayanagi, S. Ohtani, and H. A. Schuessler, Characterization of ion coulomb crystals in a linear paul trap, Phys. Rev. A **81**, 013420 (2010).

[30] M. K. Ivory, A. Kato, A. Hasanzadeh, and B. B. Blinov, A paul trap with sectored ring electrodes for experiments with two-dimensional ion crystals, Rev. Sci. Instrum. **91**, 053201 (2020).

[31] See Supplemental Material at http://link.aps.org/supplemental/10.1103/PhysRevLett.131.083602, which include Refs. [32–36], for a description of the experimental techniques used in this work, including the Paul trap, and the ions' production, cooling, and imaging. The document also provides a detailed description of the image analysis and the Monte Carlo simulations used to model the experimental data and extract the angular temperature of the ions.

[32] P. Richerme, Two-dimensional ion crystals in radio-frequency traps for quantum simulation, Phys. Rev. A **94**, 032320 (2016).

[33] M. G. Moore and R. Blümel, Prediction of an alignment transition region of two-ion crystals in a paul trap, Phys. Rev. A **50**, R4453 (1994).

[34] G. Leschhorn, T. Hasegawa, and T. Schaetz, Efficient photoionization for barium ion trapping using a dipole-allowed resonant two-photon transition, Appl. Phys. B **108**, 159 (2012).

[35] U. Dammalapati, S. De, K. Jungmann, and L. Willmann, Isotope shifts of 6s5d3d-6s6p1p1 transitions in neutral barium, Eur. Phys. J. D **53**, 1 (2009).

[36] P. Bowe, L. Hornekær, C. Brodersen, M. Drewsen, J. S. Hangst, and J. P. Schiffer, Sympathetic Crystallization of Trapped Ions, Phys. Rev. Lett. **82**, 2071 (1999).

[37] D. Leibfried, R. Blatt, C. Monroe, and D. Wineland, Quantum dynamics of single trapped ions, Rev. Mod. Phys. **75**, 281 (2003).

[38] E. Perego, L. Duca, and C. Sias, Electro-optical ion trap for experiments with atom-ion quantum hybrid systems, Appl. Sci. **10**, 2222 (2020).

[39] K. Abich, A. Keil, D. Reiss, C. Wunderlich, W. Neuhauser, and P. E. Toschek, Thermally activated hopping of two ions trapped in a bistable potential well, J. Opt. B **6**, S18 (2004).

[40] J. W. Emmert, M. Moore, and R. Blümel, Prediction of a deterministic melting transition of two-ion crystals in a paul trap, Phys. Rev. A **48**, R1757 (1993).

[41] D. J. Berkeland, J. D. Miller, J. C. Bergquist, W. M. Itano, and D. J. Wineland, Minimization of ion micromotion in a paul trap, J. Appl. Phys. **83**, 5025 (1998).

[42] L. L. Yan, W. Wan, L. Chen, F. Zhou, S. J. Gong, X. Tong, and M. Feng, Exploring structural phase transitions of ion crystals, Sci. Rep. **6**, 21547 (2016).

[43] A. Kato, A. Goel, R. Lee, Z. Ye, S. Karki, J. J. Liu, A. Nomerotski, and B. B. Blinov, Two-tone doppler cooling of radial two-dimensional crystals in a radio-frequency ion trap, Phys. Rev. A **105**, 023101 (2022).

[44] V. Golubnychiy, P. Ludwig, A. Filinov, and M. Bonitz, Controlling intershell rotations in mesoscopic electron clusters, Superlattices Microstruct. **34**, 219 (2003).

[45] M. Bonitz, V. Golubnychiy, A. Filinov, and Y. Lozovik, Single-electron control of Wigner crystallization, Microelectron. Eng. **63**, 141 (2002).

[46] M. Hirano and K. Shinjo, Atomistic locking and friction, Phys. Rev. B **41**, 11837 (1990).

[47] O. Rancova, E. Anisimovas, and T. Varanavičius, Structural transitions in laterally compressed two-dimensional coulomb clusters, Phys. Rev. E **83**, 036409 (2011).

[48] J. Kiethe, L. Timm, H. Landa, D. Kalincev, G. Morigi, and T. E. Mehlstäubler, Finite-temperature spectrum at the symmetry-breaking linear to zigzag transition, Phys. Rev. B **103**, 104106 (2021).

[49] S. Fishman, G. De Chiara, T. Calarco, and G. Morigi, Structural phase transitions in low-dimensional ion crystals, Phys. Rev. B **77**, 064111 (2008).

[50] S. Ulm, J. Rossnagel, G. Jacob, C. Degünther, S. T. Dawkins, U. G. Poschinger, R. Nigmatullin, A. Retzker, M. B. Plenio, F. Schmidt-Kaler, and K. Singer, Observation of the Kibble–Zurek scaling law for defect formation in ion crystals, Nat. Commun. **4**, 2290 (2013).

[51] K. Pyka, J. Keller, H. L. Partner, R. Nigmatullin, T. Burgermeister, D. M. Meier, K. Kuhlmann, A. Retzker, M. B. Plenio, W. H. Zurek, A. del Campo, and T. E. Mehlstäubler, Topological defect formation and spontaneous symmetry breaking in ion coulomb crystals, Nat. Commun. **4**, 2291 (2013).

[52] C. Champenois, M. Marciante, J. Pedregosa-Gutierrez, M. Houssin, M. Knoop, and M. Kajita, Ion ring in a linear multipole trap for optical frequency metrology, Phys. Rev. A **81**, 043410 (2010).

[53] H.-K. Li, E. Urban, C. Noel, A. Chuang, Y. Xia, A. Ransford, B. Hemmerling, Y. Wang, T. Li, H. Häffner, and X. Zhang, Realization of Translational Symmetry in Trapped Cold Ion Rings, Phys. Rev. Lett. **118**, 053001 (2017).

[54] E. Urban, N. Glikin, S. Mouradian, K. Krimmel, B. Hemmerling, and H. Haeffner, Coherent Control of the Rotational Degree of Freedom of a Two-Ion Coulomb Crystal, Phys. Rev. Lett. **123**, 133202 (2019).

[55] W. C. Campbell and P. Hamilton, Rotation sensing with trapped ions, J. Phys. B **50**, 064002 (2017).

[56] B. Horstmann, B. Reznik, S. Fagnocchi, and J. I. Cirac, Hawking Radiation from an Acoustic Black Hole on an Ion Ring, Phys. Rev. Lett. **104**, 250403 (2010).

[57] C. F. Roos, A. Alberti, D. Meschede, P. Hauke, and H. Häffner, Revealing Quantum Statistics with a Pair of Distant Atoms, Phys. Rev. Lett. **119**, 160401 (2017).

[58] A. Bylinskii, D. Gangloff, I. Counts, and V. Vuletić, Observation of aubry-type transition in finite atom chains via friction, Nat. Mater. **15**, 717 (2016).

[59] J. Kiethe, R. Nigmatullin, D. Kalincev, T. Schmirander, and T. Mehlstäubler, Probing nanofriction and aubry-type signatures in a finite self-organized system, Nat. Commun. **8** (2017).

[60] F. Bolton and U. Roessler, Classical model of a Wigner crystal in a quantum dot, Superlattices Microstruct. **13**, 139 (1993).